Nitrous oxide measurements in the eastern tropical South Pacific

Bachelorarbeit

im Fach Chemie

mit dem Abschlussziel Bachelor of Science

der Mathematisch-Naturwissenschaftlichen Fakultät

der Christian-Albrechts-Universität zu Kiel

vorgelegt von

Marei Pohlmann

(MtkNr.: 1135266)

Erstgutachter: Prof. Dr. Hermann W. Bange

Zweitgutachter: Dr. Damian L. Arévalo-Martínez

Abstract

Nitrous oxide (N_2O) has a major impact on global warming, as it is one of the strong greenhouse gases. The oceans are a source for N_2O to get in the atmosphere, therefore periodical observational measurements of N_2O help monitor the amount of N_2O being released into the atmosphere. Samples, which were taken on the research vessel RV SONNE in January 2022 from 2°N to 3°S in the Eastern tropical South Pacific, were analyzed with a gas chromatograph in the laboratory. To get a better understanding of the conditions in the water, data from the same area from the years 2009, 2012, 2015, and 2017 were compared with the data from 2022. Further, it was analyzed to which extend the concentration of N_2O in the water is influenced by El Niño and La Niña events, due to poor mixing of the water column during El Niño and better mixing during La Niña. The results show that the saturation and the N_2O concentration maximum were the highest in 2015, a strong El Niño year, indicating that El Niño does have an impact on the distribution and concentration of N_2O in the water column of the eastern tropical South Pacific. The impact of La Niña events in N_2O distribution was less clear.

Zusammenfassung

Distickstoffmonoxid (N_2O) hat einen starken Einfluss auf die globale Erwärmung, da es ein starkes Treibhaus Gas ist. Die Ozeane sind Quellen, durch die N_2O in die Atmosphäre gelangt, deshalb helfen regelmäßige Messungen die Menge an N_2O zu kontrollieren, die in die Atmosphäre abgegeben wird. Wasserproben wurden auf dem Forschungsschiff RV SONNE im Januar 2022 von 2°N bis 3°S im östlichen tropischen Südpazifik entnommen und im Labor mit einem Gaschromatographen analysiert. Um ein besseres Verständnis von den Bedingungen im Wasser zu erhalten, wurden Daten aus dem gleichen Gebiet von 2009, 2012, 2015 und 2017 mit denen aus 2022 verglichen. Weiterhin wurde geschaut, ob El Niño und La Niña Ereignisse einen Einfluss auf die Konzentration von N_2O im Wasser haben, aufgrund von einer geringeren Durchmischung der Wassersäule während El Niño und einer stärkeren Durchmischung während La Niña. Die höchsten Werte für Sättigung und das Konzentrationsmaximum von N_2O wurden für 2015 gefunden, einem starken El Niño Jahr, was auf einen Einfluss von El Niño auf die Verteilung und Konzentration von N_2O in der Wassersäule hinweist. Für La Niña konnten keine klaren Indikatoren gefunden werden.

Table of contents

1. Introduction

Nitrous oxide (N_2O) is a long-living atmospheric greenhouse gas, which effects the stratospheric ozone depletion. In the ocean N_2O is produced through nitrification and denitrification. Their interaction with the marine system is important for understanding global climate change, as almost one-third of N_2O is emitted by the oceans. The eastern tropical South Pacific is a region with a high sea-to-air flux of N_2O, therefore, a periodic measurement in the area helps predict the amount of N_2O being released into the atmosphere. (Bakker et al. 2014; Ji et al. 2019)

The research vessel SONNE was going from Las Palmas to Guayaquil in Ecuador, which took place from 11.12.2021 to 11.01.2022 (Quack 2022). Even though samples for N_2O and Methane (CH_4) were taken the entire cruise, the following will focus on the N_2O samples of stations 33 to 36, which are located in the eastern tropical South Pacific. The samples were analyzed using a gas chromatograph. Afterwards, the data was evaluated and compared with data from the same area in 2009, 2012, 2015, and 2017.

The eastern tropical South Pacific holds one of the major upwelling systems and is known for the El Niño-Southern Oscillation (ENSO), which consists of the El Niño, the La Niña and the neutral phase. The El Niño implies a warming of the rather cold surface water, compared to other equatorial regions. During the La Niña the surface water temperature is lower than in the neutral phase. The ENSO has a major impact on the climate as it can be the origin of rainfall and droughts (Ji et al. 2019).

The measurements taken in this area over the years help predict the amount of N_2O being emitted into the atmosphere in the eastern tropical South Pacific and the possible impact the ENSO has on the concentration of N_2O in the water column. Therefore, this thesis will look at the impact the ENSO might have on the N_2O concentration in the water column, due to poor mixing during El Niño and better mixing during La Niña.

2. Theoretical background

2.1. Nitrogen cycle

N_2O is a main component in the oceanic nitrogen cycle and is produced by bacteria and archaea through nitrification and denitrification. As the formation of N_2O is dependent on the presence of dissolved oxygen (O_2), nitrification takes place in oxic conditions and in hypoxic conditions N_2O is mainly formed through denitrification (Bakker et al. 2014).

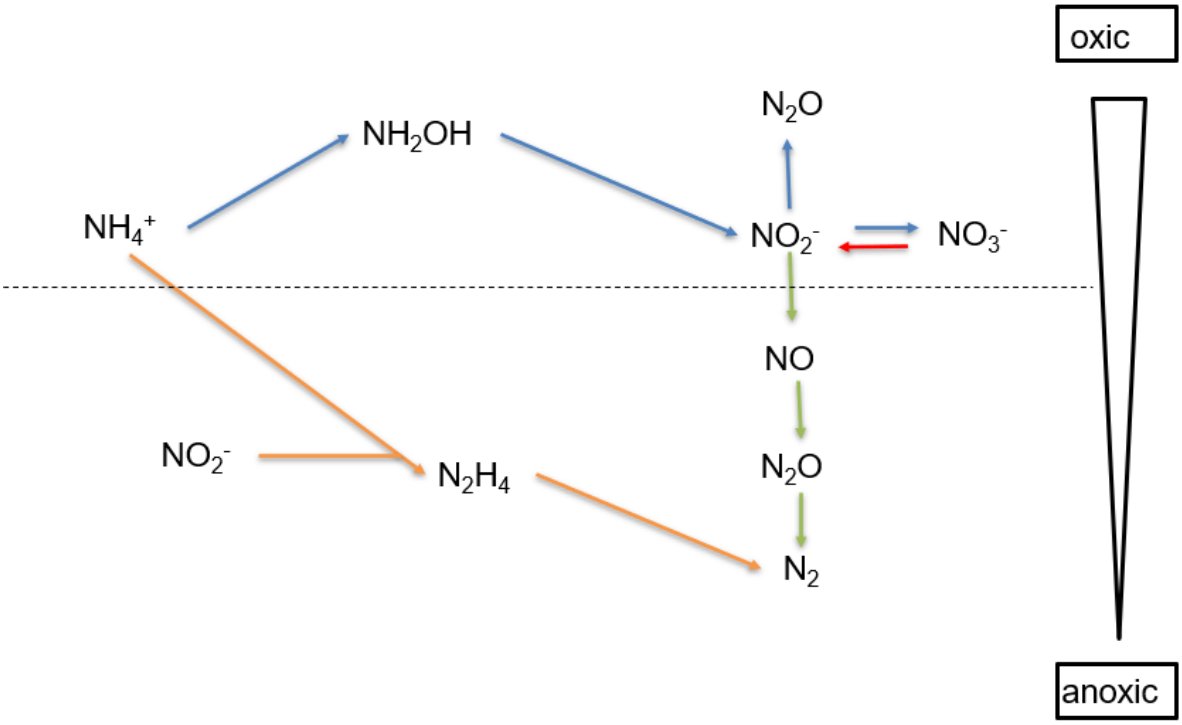

Fig. 1: Schematic representation of the nitrogen cycle in the ocean, on the right a vertical oxygen gradient is shown. The blue arrows represent nitrification, red is the reduction of nitrate, denitrification is represented by green, and orange shows anammox. The oxycline is represented by the dotted line (Bakker et al. 2014).

Nitrification is described as the process of which fixated nitrogen, ammonium (NH_4^+) is being oxidized to nitrate (NO_3^-) by bacteria and archaea. N_2O is produced as a by-product during the two-step metabolism of ammonia. In the first step, ammonia-oxidizing bacteria transform NH_4^+ into hydroxylamine (NH_2OH) and in the second step, NH_2OH is oxidized to nitrite (NO_2^-) and then NO_3^-. For the oxidation of NH_3 to NH_2OH

two electrons are required for water to be formed. These electrons are gained from the second step, where four electrons are released (Arp 2009; Wrage et al. 2001; Bakker et al. 2014).

When O_2 is less available, bacterial and archaeal denitrifiers use NO_3^- instead of O_2 as an electron acceptor and, therefore, reduce NO_3^- in four steps to N_2, this process is called denitrification. The intermediates are NO_2^-, nitric oxide (NO), and N_2O as shown in Figure 1. N_2O is not produced as a by-product, yet it is an intermediate of denitrification reduction. Whether N_2O is produced or consumed is dependent on the O_2 concentration. Denitrification can still influence the amount of greenhouse gas in the atmosphere if it is available in high concentrations (Bakker et al. 2014; Wrage et al. 2001).

Nitrifier denitrification is the process of ammonia oxidation, followed by denitrification. This is limited to autotrophic NH_3-oxidizers and contains of the oxidation of NH_3 to NO_2^- and the reduction of NO_2^- to N_2 (Wrage et al. 2001; Bakker et al. 2014).

The anaerobic ammonium oxidation (anammox) also takes place in the oxygen minimum zone (OMZ). Thereby NH_4^+ reacts with NO_2^- to N_2. Only a specific kind of bacteria can reduce NH_4^+ in this way, as they possess an organelle, the anammoxome, which is distinctive for their kind (Devol 2015).

To indicate the production of N_2O, ΔN_2O (Equation 1) is plotted against the apparent oxygen utilization (AOU). AOU (Equation 2) can be seen as the concentration of O_2 that is used up during remineralization, for a higher AOU value less O_2 and more N_2O is apparent in the water. A positive ΔN_2O represents the excess of N_2O, therefore a positive correlation of the two parameters shows the production of N_2O through nitrification. A negative ΔN_2O indicates a lower concentration of N_2O in the water than in the atmosphere. Is the concentration of N_2O in the surface water higher than in the atmosphere, N_2O is dispensed in the atmosphere, as the ocean and atmosphere equilibrate gases (Walter et al. 2006; Ji et al. 2019).

The following equation was used to calculate ΔN_2O:

$$\Delta N_2O\ (nmol\ L^{-1}) = N_2O_{(observed)} - N_2O_{(equilibrium)} \quad (1)$$

AOU is defined as:

$$AOU\ (\mu mol\ kg^{-1}) = AOU_{(equilibrium)} - AOU_{(observed)} \quad (2)$$

2.2. Eastern tropical South Pacific

The coasts of Peru and Chile hold one of the main upwelling systems, the Humboldt Current System, and a major OMZ. It extends from ~ 45°S, on the south coast of Chile to ~ 4°S, on the northern coast of Peru. Strong winds blow in the direction of the equator parallel to the coast, which causes horizontal divergence. Therefore, the subsurface water rises to the surface and replaces the previous surface water. The upwelling area can be divided into three areas, the first being in central-southern Chile with a seasonal upwelling, the second has lower productivity than the first one in northern Chile and southern Peru, and the third is in front of Peru, productive all year long. An overview of the seasonal and permanent upwelling can be seen in Figure 2. The upwelling is experienced the whole year because of unusual winds, the permanent South Pacific High in northern Chile, and the low-pressure Region in Indonesia (Montecino and Lange 2009).

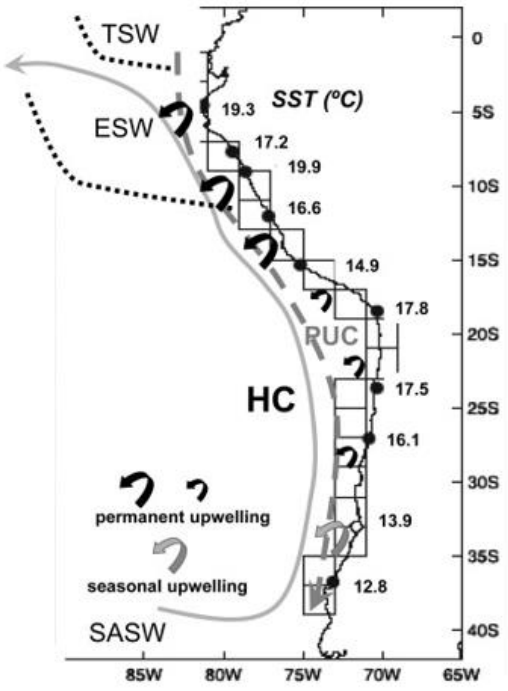

Fig. 2: The Humboldt Current (HC), grey arrows represent seasonal upwelling and black arrows permanent upwelling. The average sea surface temperature (SST) is given in °C , further the Poleward Undercurrent (PUC), the Tropical Surface Waters (TSW), the Equatorial Surface Waters (ESW) and the Sub-antarctic Surface Waters (SASW) are plottet (Montecino and Lange 2009).

The Humboldt Current System consists of several different currents. The cold Sub-Antarctic Surface Water flows northwards of ~ 45°S and is also known as the Peru-Chile Current (Figure 2). In the north, the cold upwelled water collides with the Tropical Surface Waters. The equatorial undercurrent feeds the Peru-Chile Countercurrent, which flows opposite the Sub-Antarctic Surface Water along the coastline (Montecino and Lange 2009).

The El Niño is an event that takes place in the Peruvian coastal area and has a global impact as it can cause major droughts or rainfall. Due to the connection between the ocean and the atmosphere, it is also referred to as ENSO. ENSO describes a warming of the sea surface temperature (SST), which takes place around Christmas. In comparison to other regions near the equator, the eastern equatorial Pacific is rather cold, which is caused by the constant upwelling from the cold deep waters. The SST at the equatorial gradient is warmer in the west, which is causing the Walker Circulation, a thermodynamic circulation parallel to the equator. The cold, dry air from the east is pushed to the west, where it is heated up and able to absorb moisture. The westward wind is compensated by pressure gradients. In the west the warm water is building up leading to the thermocline being at 100 m to 200 m beneath the surface. The thermocline rises in the east, because of the Coriolis effect, as it rotates the flow direction of the water north and south, which allows the cold water to rise to the surface. This combined with the upwelling is the reason for the cold water in the eastern equatorial Pacific. If the Walker Circulation slowed down or stopped, it is likely for the ENSO to take place (Cane 1986; Neelin and Latif 1998). The ENSO can be divided into three sections, El Niño, La Niña, and a neutral phase. A higher SST is a significant indication for the El Niño phase, and a lower SST for the La Niña. During the neutral phase, the SST is at a normal level (Ji et al. 2019).

3. Methods

3.1. Sample extraction

The samples were taken during the transit of RV SONNE from 11.12.2021 to 11.01.2022. The cruise started in Las Palmas and ended in Guayaquil, Ecuador. It is part of the SO287-CONNECT, an international collaboration of GEOMAR, Hereon, and the University of Bremen (Quack 2022). With the help of CTD-Niskin bottles, three samples were collected at each sampling station at different depths, which were for the Day-sampling 6 m, 50 m, the deep chlorophyll maximum, 200 m, the OMZ, and 1000 m. The samples that were gathered at night, were collected at the depths of the samples taken at day, except for 1000 m the samples were taken at 2000 m. There were two additional depths, that are, 3500 m, and bottom water. The triplicate samples were then transferred into 20 mL vials made from brown glass. To not get air bubbles stuck inside the vials, they were rinsed with around 40 mL of the sample and immediately covered with butyl rubber stoppers and aluminum caps. 50 µL of oversaturated mercury chloride solution ($HgCl_2$) was injected to preserve the sample and avoid further microbial N_2O consumption or production. The vials were then stored upside down in a dark room at room temperature and shipped to Germany for further analyses.

3.2. Gas chromatography

Gas chromatography (GC) is used to identify and quantify substances. The GC consists of a column through which a gas is constantly flowing, this gas is called the mobile phase. The gas comes from a high-pressure gas tank and runs towards the low-pressure end of the column, where the detector is located. The mobile phase ensures that the injected gas is carried through the column. The walls of the column have a 0,25-5 µm thick layer of polymer, which is the stationary phase of the GC. The column has an average length of 10 to 60 m. The molecules passing through the column have intermolecular interactions with the stationary phase, which is different for every molecule. This varying partitioning behavior leads to different times the molecules spend in the column, which is called retention time. Therefore, they can be separated and specified as to which molecules they are (Vitha 2016).

An Electron Capture Detector (ECD) is used to identify the N_2O at the end of the column. This type of detector works efficiently with molecules that have high electronegativity and polyhalogenated organic compounds. A radioactive source, normally a curved nickel sheet covert with ^{63}Ni, is used to produce electrons. The mobile phase passes this stream of β radiation and forms ions and electrons.

$$G \rightarrow G^+ + e^- \quad (3)$$

The resulted ions move to a collector electrode and form a basic ionization current. The electrons can bond with molecules.

$$M + e^- \rightarrow M^- \quad (4)$$

Because of the absent of those electrons the basic ionization current becomes smaller, and serves as the signal (Vitha 2016; Kolb 2003).

3.3. Analysis in the laboratory

In the laboratory, these samples were analyzed using the Hewlett-Packard 5890 Series II, Agilent Technologies GC (Kock et al. 2016). Before the samples could be analyzed the vials were checked for small air bubbles as they could potentially be causing differences in the data. The N_2O samples were prepared for the gas chromatograph by using a static equilibration method. Therefore, a gas is injected on top of the liquid phase in the closed vial (Snow and Bullock 2010). For this reason, a 20 mL syringe was inserted into the sample vial, so the excess liquid sample would be able to evade into that syringe, as 10 mL Helium was injected into the vial. Afterward, the vial was firmly shaken for 20 s and then left to equilibrate for at least two hours, to provide enough time for the equilibrium between the solution and the gas phase to take place. When the headspace is equilibrated with the liquid sample the concentration of N_2O in the headspace is as well meaningful for the concentration of N_2O in the liquid sample (Snow and Bullock 2010). The N_2O samples were manually injected into the gas chromatograph-Electron Capture Detector system, which consists of a 6′ 1/8″ packed column, for the mobile phase Argon and Methane (95% and 5%) were used with 30 mL min^{-1} (Kock et al. 2016). The GC was run at 190 °C and for the recording of the peaks the computer program ChromStar 6.3 (SCPA, Germany, 2006) was used. To minimize errors during the analysis the GC was calibrated every day, therefore,

different standard gases in different concentrations were used, these can be seen in Table 1.

Tab. 1: Standard gases, their dilution factor for the calibration of the GC, and their mole fraction.

V He [mL]	V 14 [mL]	V 5B [mL]	Mole fraction N_2O [ppb]
3	6	-	237,183
-	9	-	355,775
3	-	6	696,398
-	-	9	1044,597

The concentration of N_2O was calculated through the integration of the peaks with the help of the computer program Chromstar 6.3. Afterwards, the computer program Excel was used for plotting the integrated areas against the mole fraction and a quadratic regression was performed. For further processing of the data the computer program Ocean Data View was used.
The concentration is calculated with the following equation:

$$C_{N_2O}[nmolL^{-1}] = \frac{\left(\beta \; x \; P \; V_{wp} + \frac{x \; P}{R \; T} V_{hs}\right)}{V_{wp}} \quad (5)$$

The variables used for this equation are listed in Table 2 (Walter et al. 2006).

Tab. 2: Naming the variables used in Equation 5.

Variable	name of variable
β	Bunsen solubility in nmol L^{-1} atm^{-1}
x	dry gas mole fraction of N_2O in the headspace in ppb
P	atmospheric pressure in atm
V_{wp}	volume of water phase
V_{hs}	volume of headspace phase
R	Gas constant (8.2054 x 10^{-2} L atm mol^{-1} K^{-1}
T	Temperature during equilibration

4. Results

The analyzed data from the SO287 cruise from 2022 is displayed in vertical sections and depth profiles. Furthermore, the data is compared with data from the years of 2009, 2012, 2015 and 2017, where samples were taken from the same area. More specifically, the depth-profiles, AOU data and the depth-integrated N_2O concentrations are compared. The years were chosen, as in 2009 and 2017 a La Niña event and in 2015 an El Niño event took place. 2012 is a neutral year and, therefore, it can be used to compare the data with El Niño and La Niña years.

4.1. Vertical distribution in 2022

The location of the station were the samples in the eastern tropical South Pacific in 2022 were taken are shown in Figure 3. The stations appear at a Longitude of 85°W and extend from a Latitude of 2,3°N to 2,6°S.

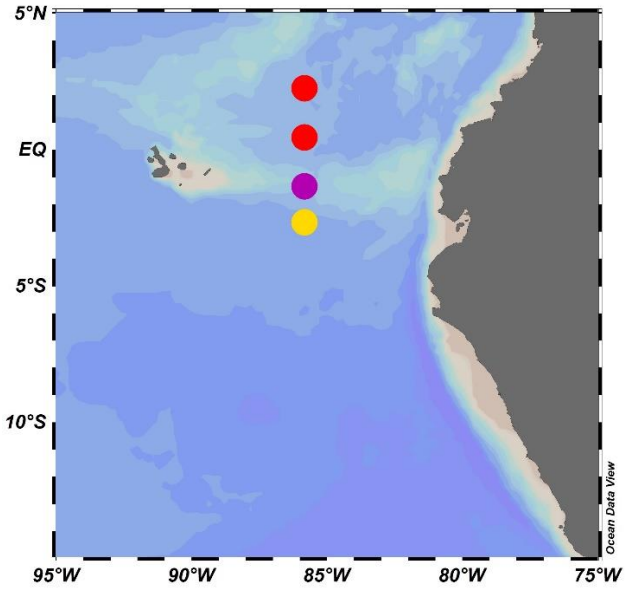

Fig. 3: Overview of the stations 33 to 36 of the year 2022. The stations from 2°N to the Equator are in red, violet is for the Latitude section from the Equator to 2°S and yellow for the section from 2°S to 4°S.

The vertical sections in Figure 4 show the concentration of N_2O, O_2, and the temperature of the water, when the samples were taken. The concentration of N_2O is lower at the surface and higher in the deeper water. For station 36, at 2.6°S the concentration maximum appears at 200 m depth and decreases faster than the other stations. For the other three stations the maximum emerges at a depth between 300 m and 400 m. For the concentration of O_2, an opposite pattern can be seen for the different stations. The concentration is high at the surface and decreases in the deeper water. Only the N_2O maximum from the station 36 cannot be seen as a O_2 minimum, the minimum at this station appears at a depth of 350 m.

The vertical sections depict the major OMZ that is typical for the eastern tropical South Pacific, as well as the colder temperature due to the upwelling (Ryabenko et al. 2012). The temperature was between 20°C and 25°C at the surface and only between 10°C and 15°C down to a depth of 500 m, the water is known to be colder in comparison to other equatorial areas (Ji et al. 2019).

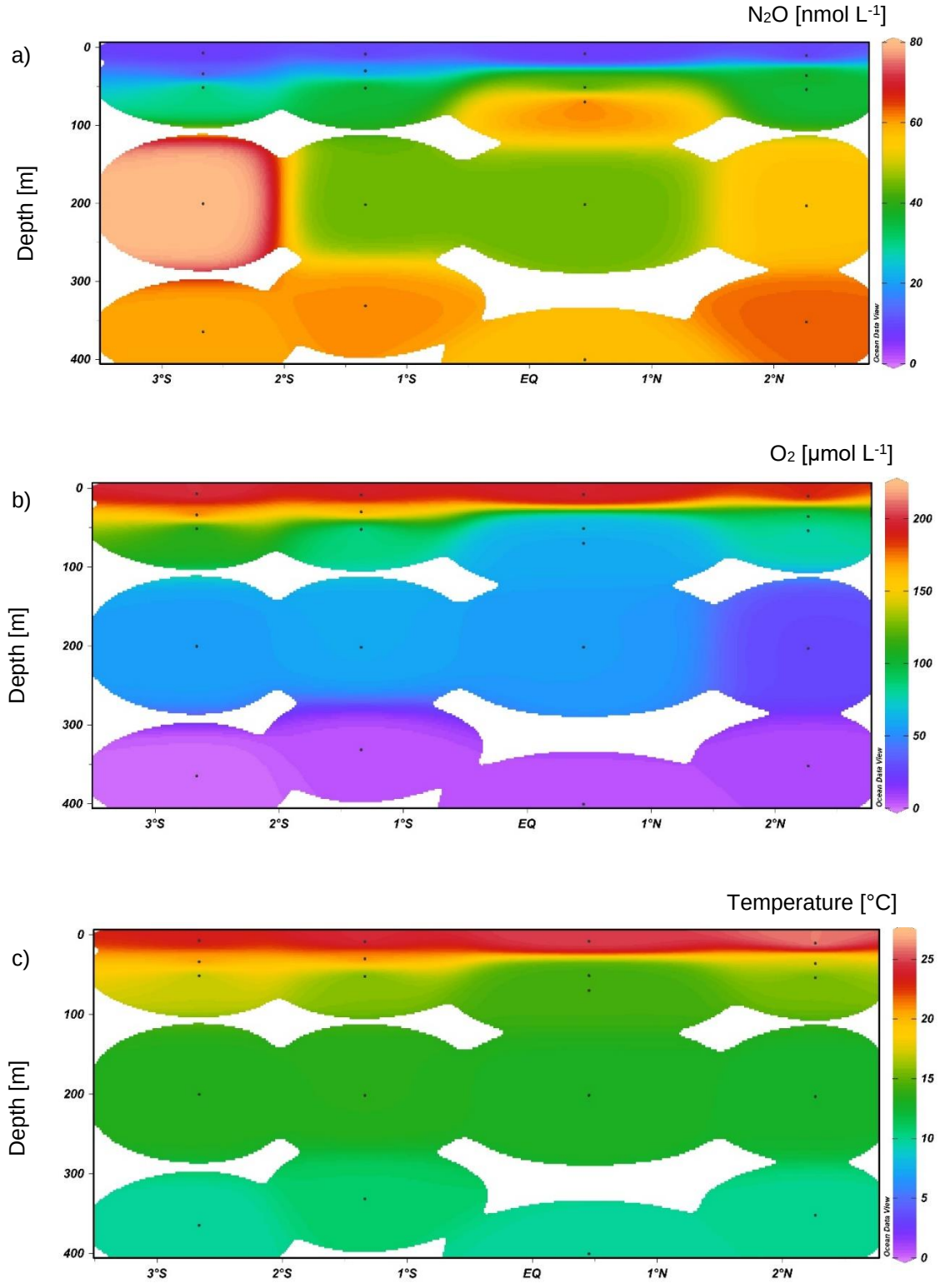

Fig. 4: vertical sections of stations 33 to 36, a) shows the concentration of N_2O in the different depths the samples were taken, b) shows the concentration of O_2 and c) the temperature of the water, when the samples were taken. The concentrations for a) and b) as well as the temperature for c) can be taken from the color scale on the right. From the left to right stations 36 to 33 are shown.

Figure 5 shows the concentration of N_2O and O_2 in relation to the depth the samples were taken at stations 33 to 36. O_2 shows similar concentrations for all four stations. The concentration falls rapidly until a depth of approximately 50 m. the concentration decreases further, yet more slowly up to a depth of 350 m and 400 m. For the concentration of N_2O, it is the other way around. The concentration increases rapidly until a depth of 50 m. Below that the concentration is still increasing however, slower, until the maximum of around 60 nmol L^{-1} is reached. Station 34 has the highest concentration of N_2O at the depth of 50 m, which is noticeable, and Station 36 has a concentration peak at a depth of 200 m. This means their concentration does not increase as steadily as in the other two stations. The two concentration profiles show an opposite pattern, the O_2 minimum is at the same depth as the N_2O maximum. Except for the two concentration peaks in station 34 and 36 mentioned before. These measures could be outliers or caused by mistakes during the sample extraction. Overall, the data shows a clear opposite pattern, which is an indicator for nitrification as the main source of N_2O in the area the samples were taken.

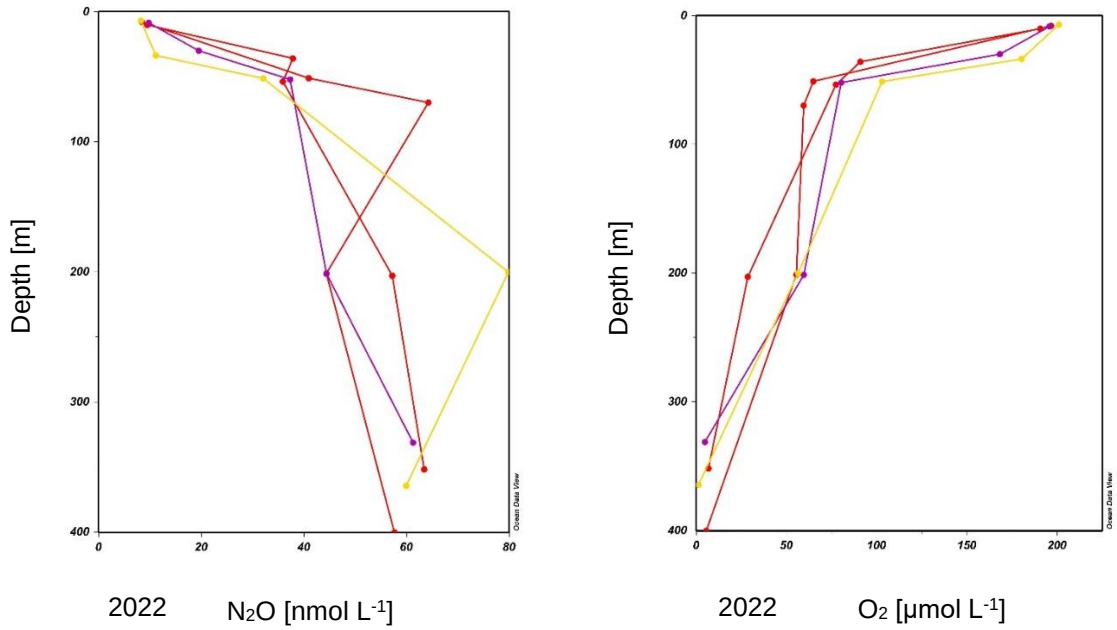

Fig. 5: Left: Depth profile of the N_2O concentration. Right: Depth profile of the O_2 concentration. The stations located in the Latitude section from 2°N to the Equator are red, from the Equator to 2°S are violet and from 2°S to 4°S are yellow.

4.2. Comparison with archived data sets

Data from the cruises M77-4 (2009), M90 (2012), SO243 (2015), and M138 (2017) is used for comparing and classifying the concentration of N_2O and O_2. Figure 6 shows the stations, where the samples were collected, which are at the same area expanding from 2°N to 6°S only in 2009 the stations reached till 14°S. The data was taken from the MEMENTO database (Data access - MEMENTO (geomar.de) last accessed: 06.08.2022).

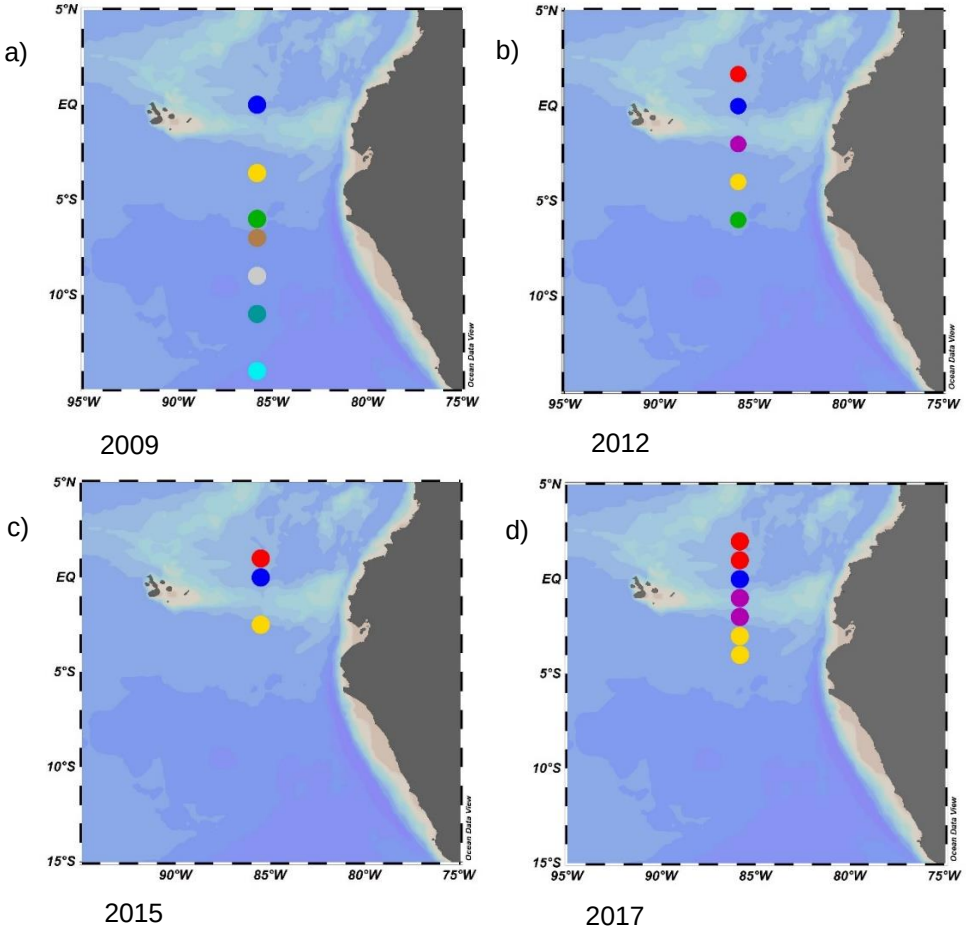

Fig. 6: Overview of the stations of the following cruises: a) M77-4 (2009), b) M90 (2012), c) SO243 (2015) and d) M138 (2017). The stations located in the Latitude section from 2°N to the Equator are red, station located on the Equator are blue, the stations located in the section from the Equator to 2°S are violet, from 2°S to 4°S are yellow, from 4°S to 6°S are green, from 6°S to 8°S are brown, from 8°S to 10°S are grey, from 10°S to 12°S are dark green and from 12°S to 14°S are light blue.

Figure 7 shows a comparison of the depth profiles for the N_2O concentration and Figure 8 the O_2 concentration for the years 2009, 2012, 2015 and 2017. The section 2°N to the equator (red) is represented in 2012, 2015, 2017 and 2022. The concentration of N_2O has its maximum of 65 nmol L^{-1} at a depth of 250 m in 2012. In 2015 the maximum of 80 nmol L^{-1} is reached at the same depth as in 2012, in 2017 the maximum of 67 nmol L^{-1} is reached at a depth of 300 m. The minimum of the concentration of O_2 is at a depth of 320 m in 2012 and 2015. For 2017 the minimum is at a depth of 300 m. Samples were taken from the equator (blue) in the years 2009, 2012, 2015 and 2017. For 2009 the maximum for the concentration of N_2O is at a depth of 300 m, the concentration is 58 nmol L^{-1}. For 2012 the maximum concentration is 65 nmol L^{-1} at a depth of 350 m, the maximum for 2015 is almost 100 nmol L^{-1} at a depth of 370 m and for 2017 the maximum is 60 nmol L^{-1} at a depth of 250 m. The concentration of O_2 shows a good opposite pattern of N_2O except of 2015, where the minimum already appears at a depth of 320 m. The section from the equator to 2°S (violet) is represented in 2012 and 2017. In 2012 the N_2O maximum of 65 nmol L^{-1} appears at a depth of 250 m and in 2017 the maximum of 70 nmol L^{-1} appears at the same depth. The concentration of O_2 shows good opposite pattern. The next section is from 2°S to 4°S (yellow) and is represented in all years. For 2009 the maximum of N_2O of 60 nmol L^{-1} at a depth of 200 m, for 2012 the same maximum concentration is found, yet at a depth of 350 m. In 2015 a maximum of almost 90 nmol L^{-1} is found at a depth of 300 m and for 2017 a concentration of 70 nmol L^{-1} is found at the same depths. The opposite pattern of O_2 and N_2O can be found in 2009, 2015 and 2017. In 2012 the minimum concentration of O_2 can already be found at a depth of 250 m. The section from 4°S to 6°S (green) can be found in 2009 and 2012. In 2009 the N_2O concentration maximum of 60 nmol L^{-1} appears at a depth of 200 m and in 2017 the maximum of almost 70 nmol L^{-1} is found at the same depth. 2009 was the only year where samples at the locations 7°S, 9°S, 11°S and 14°S were taken, therefore, they are not compared with the other years. Overall, the highest N_2O concentrations are found in 2015, the concentration maxima are found between a depth of 200 m and 300 m in every year.

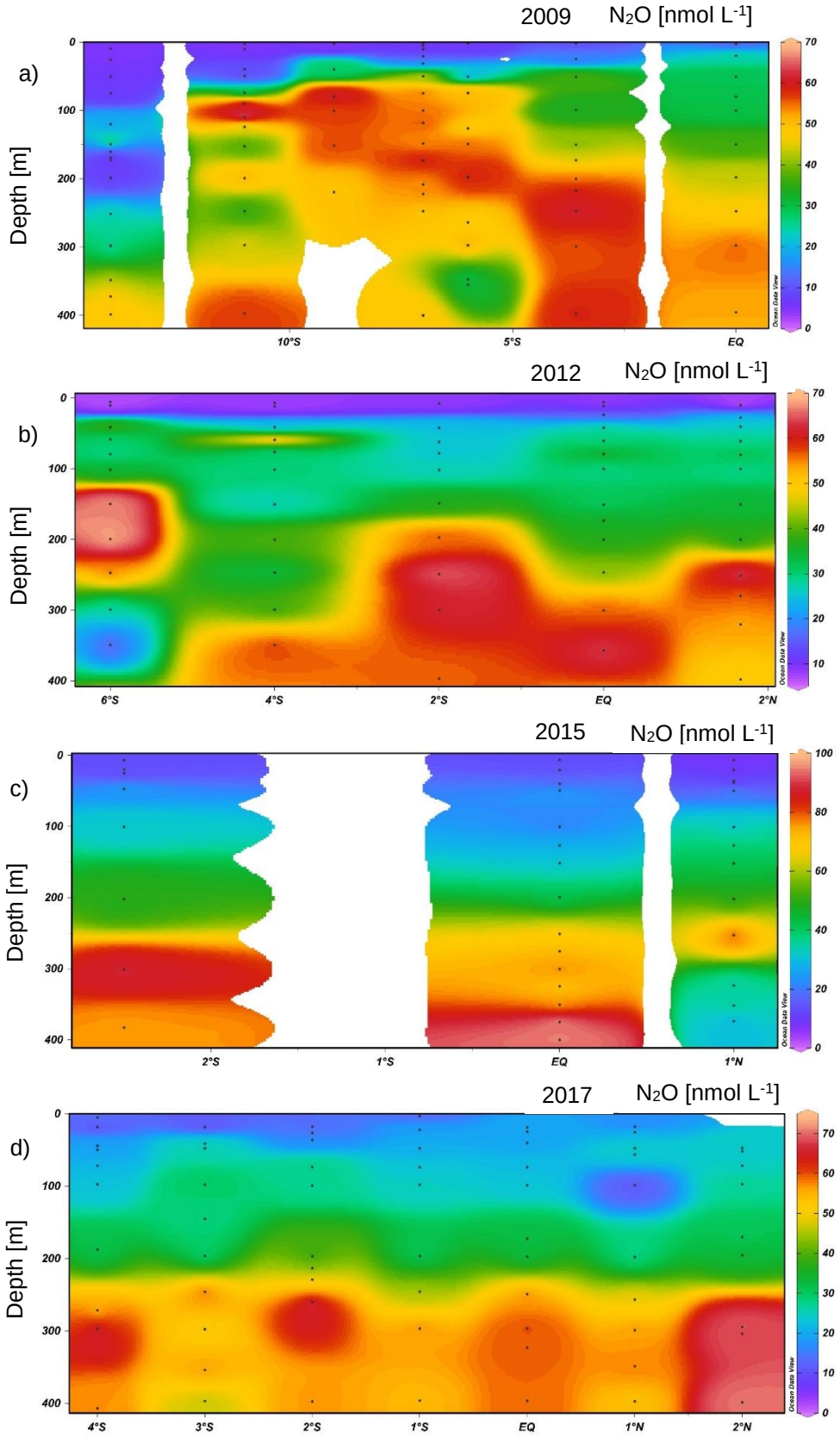

Fig. 7: Vertical sections of the N_2O concentrations until a depth of 400 m for the years a) 2010, b) 2012, c) 2015 and d) 2017.

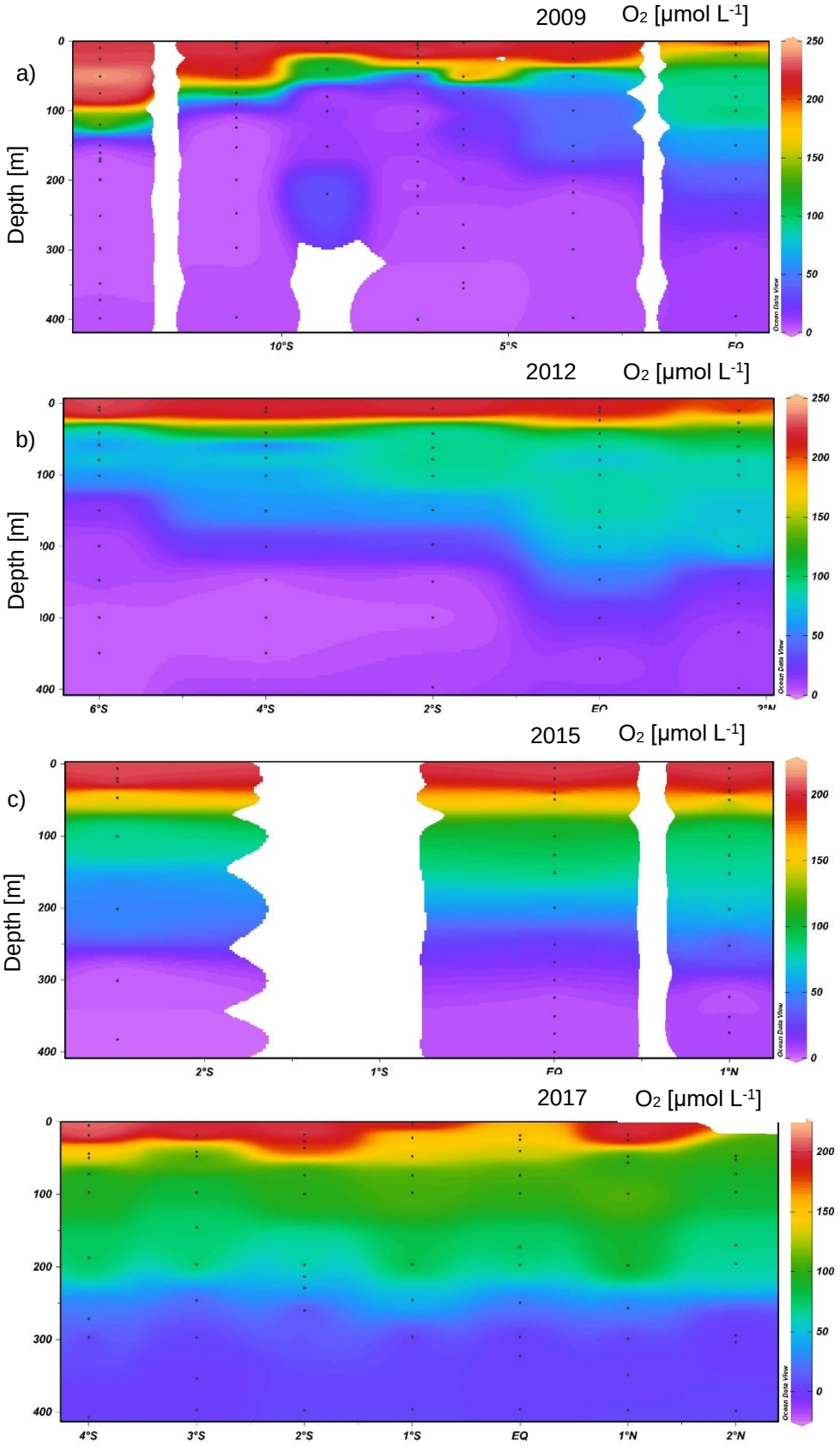

Fig. 8: Vertical sections of the O_2 concentrations until a depth of 400 m for the years a) 2010, b) 2012, c) 2015 and d) 2017.

Figure 9 shows AOU plotted against ΔN_2O for the years 2009, 2012, 2015, 2017 and 2022. ΔN_2O was calculated with Equation 1. For $N_2O_{(observed)}$ the measured concentration from the stations was added to the equation, for $N_2O_{(equilibrium)}$ data from the NOAA database was used. The station Tutuila, American Samoa (14,25°S; 170,56°W) was chosen, as it was the closest station with current data available. The most current data from closer stations, for example the Easter Island, Chile, was from 2019, therefore the station was not chosen. The most current data from Tutuila was from December 2021, which was used for the cruise SO287, even though the samples were taken in January 2022. Table 3 shows the mole fraction in parts per billion (ppb) that was used to calculate ΔN_2O and AOU. AOU was calculated with the help of the computer program Ocean Data View.

In the plot only the data until a depth including the OMZ was plotted as the data beneath the OMZ would result in a different gradient of the linear regression. A positive linear regression, which can be seen for all five years, indicates an N_2O production through nitrification. 2009 is the only year with negative AOU values and ΔN_2O being between 0 nmol L^{-1} and 10 nmol L^{-1}. The data scatters at around 250 µmol L^{-1}, as the gradient is different for the OMZ. This indicates a N_2O consumption for water where the O_2 concentrations are lower than 5 µmol L^{-1} (Ryabenko et al. 2012). The gradient for each year varies, 2009 has a gradient of 0,1278 nmol µmol^{-1}, 2012 0,1455 nmol µmol^{-1}, 2015 0,1985 nmol µmol^{-1}, 2017 0,1614 nmol µmol^{-1} and 2022 0,2149 nmol µmol^{-1} (Figure 17 Appendix). A higher gradient means that more N_2O is produced through nitrification. Therefore, each year more N_2O is produced, except 2017, where the gradient is lower than 2015 and the highest gradient is found in 2022. These gradients are comparable with data from literary, for north Chile (21°S) a gradient of 0,18 nmol µmol^{-1} is mentioned (Farías et al. 2007). Furthermore, an average gradient of 0,13 nmol µmol^{-1} for cruises in 2009 and 2012 off Peru was evaluated in 2016 (Kock et al. 2016). In 2009 a gradient of 0,30 nmol µmol^{-1} was evaluated, where only O_2 concentrations between 5 and 50 µmol L^{-1} were included (Ryabenko et al. 2012).

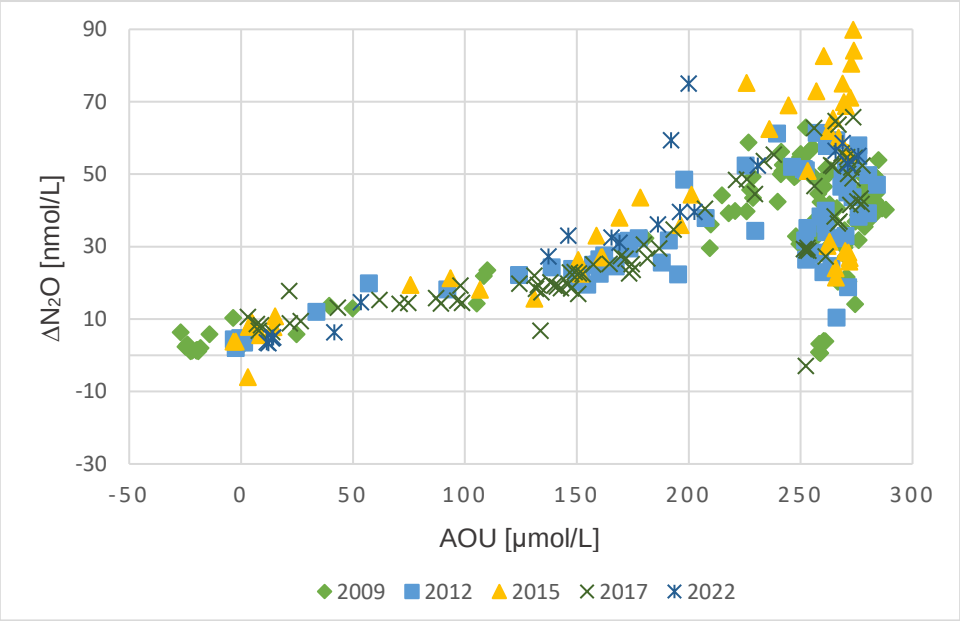

Fig. 9: Plot of AOU and ΔN_2O for 2009 (light green rhombus), 2012 (light blue square), 2015 (yellow triangle), 2017 (dark green cross) and 2022 (dark blue cross).

Tab. 3: shows the mole fraction of N_2O in the atmosphere in ppb, measured at the station Tutuila, American Samoa (14,25°S; 170,56°W), as well as the year and month the measurements were taken. The data was downloaded from: https://gml.noaa.gov/aftp/data/trace_gases/n2o/flask/surface/txt/n2o_smo_surface-fla sk_1_ccgg_event.txt (last access: 08.08.2022)

Cruise	Year	Month	N_2O (atmosphere) [ppb]
M77-4	2009	01	322.45
M77-4	2009	02	321.51
M90	2012	11	325,34
SO243	2015	10	328,27
M138	2017	06	328,64
SO287	2021	12	334,98

4.3.1. Influence of ENSO in N_2O distribution

The Ocean Niño Index (ONI) evaluates the progress and strength of the ENSO, it is defined as the average three-month SST anomalies in the Niño region (5°N-5°S, 120°-170°W). El Niño events consist of SST anomalies > 0,5°C and La Niña events < -0,5°C (José et al. 2019). The data is shown in Figure 10, for the years 2009, 2012, 2015, 2017, and 2022. For the cruise SO287 in 2022 only data for the first six months was available at the time it was accessed. 2009 starts with the first three months being lower than -0,5°C, then it rises throughout the year with the highest temperature being 1,6°C in December. The samples were taken in January and February with -0,8°C. 2012 starts with the first three months being < -0,5°C and the other month being neutral ranging between -0,5°C and 0,5°C. The samples were taken in November of 2012 with an ONI of 0,1°C. In 2015 a strong El Niño event took place, the data shows the year being 0,5°C for the first three months and a further increasing of the data until the peak of 2,6°C in November and December. 2017 has a neutral ONI except for the last three months of the year which is < -0,5°C with the peak in December being -1,0°C. 2022 shows < -0,5°C for the first 6 months of the year around -1,0°C, indicating a La Niña.

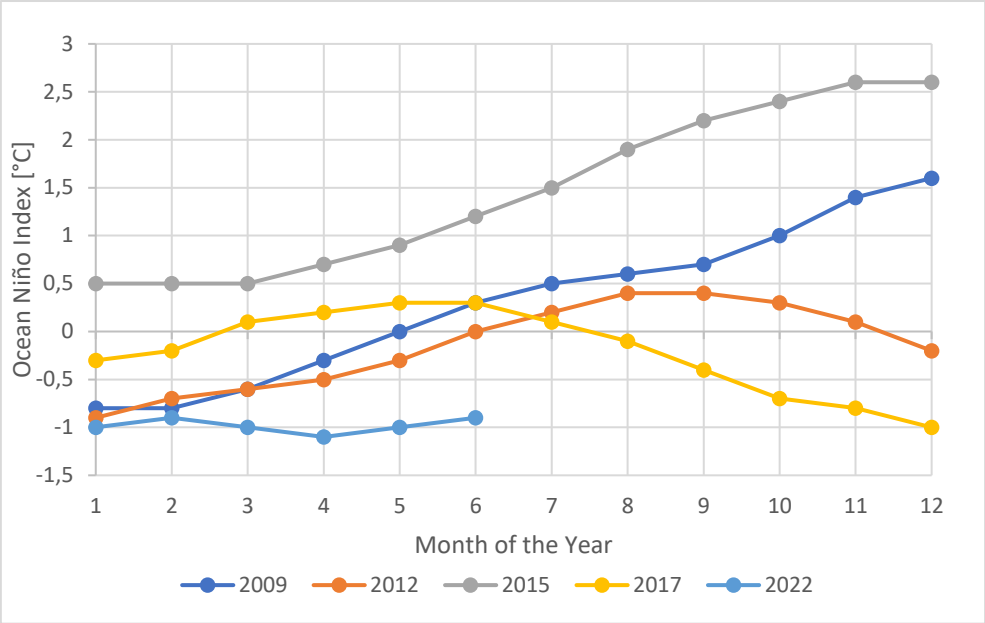

Fig. 10: Ocean Niño Index for the years 2009 (dark blue), 2012 (orange), 2015 (grey), 2017 (yellow) and 2022 (light blue). The data was downloaded from https://origin.cpc.ncep.noaa.gov/products/analysis_monitoring /ensostuff/ONI_v5.php (last access: 18.08.2022).

El Niño and La Niña events are noticeable through warmer (El Niño) and colder (La Niña) surface waters. In Figure 11, the water temperature for the years 2009, 2012, 2015, and 2017 is displayed. In 2009 and 2015 the highest surface temperatures of over 25°C were measured. Furthermore, in 2015 the warm water of around 25°C extends to a depth of approximately 50 m and from 50 m to approximately 75 m a temperature of 20°C was measured. 2017 holds the lowest surface temperature of approximately 20°C and 25°C measured at the station located 1°N. The warm water extends to a depth of 25 m to 50 m and, therefore, the temperature shows La Niña characteristics. The surface temperature of 2012 is between the surface temperatures of 2009 and 2017. 2022 temperatures of 25°C were measured at the surface and it extends until a depth of approximately 50 m, it shows resemblance with the vertical section of 2009.

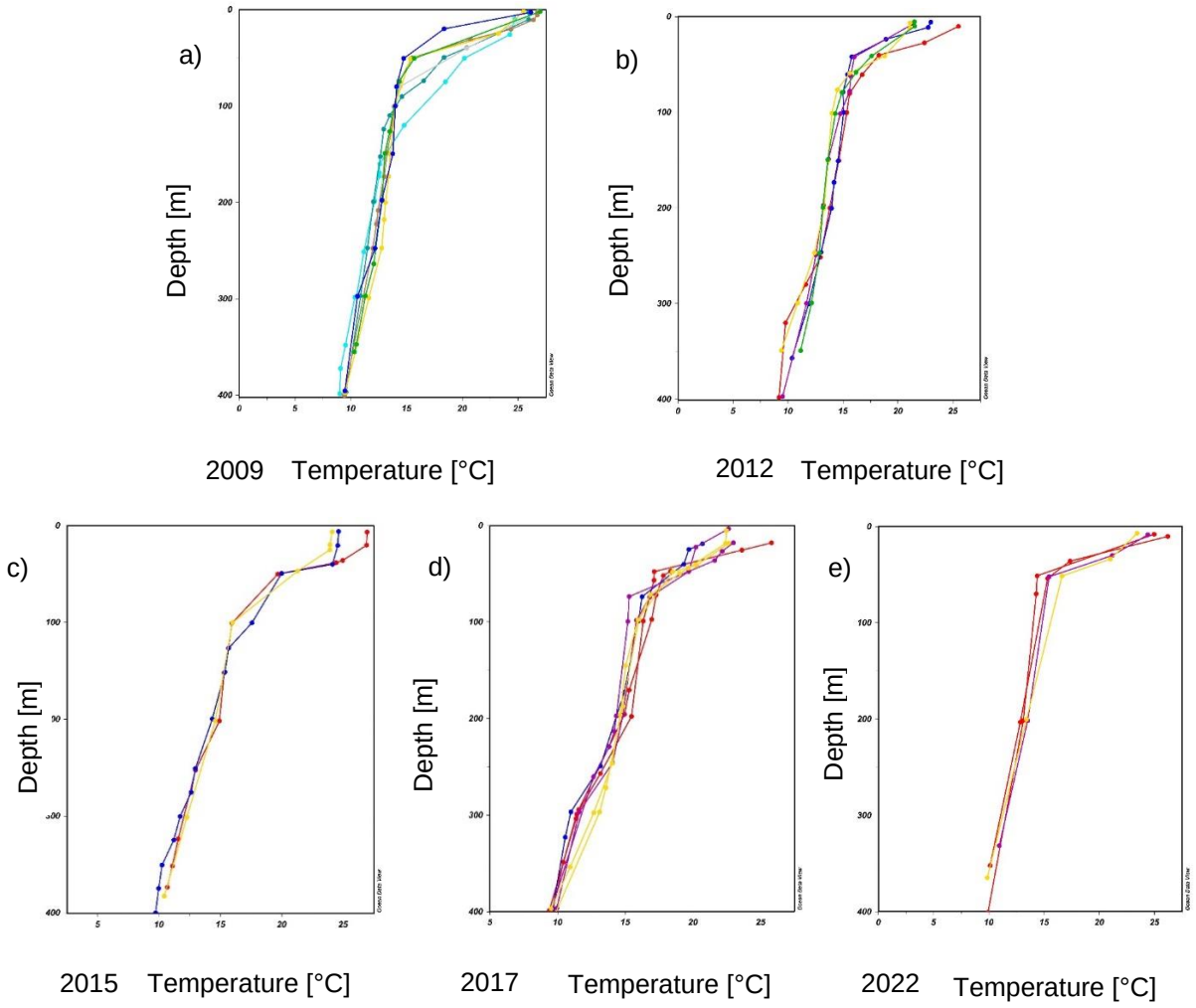

Fig. 11: Depth profiles of the years a) 2009, b) 2012, c) 2015, d) 2017 and e) 2022 showing the temperature. The stations located in the Latitude section from 2°N to the Equator are red, station located on the Equator are blue, the stations located in the section from the Equator to 2°S are violet, from 2°S to 4°S are yellow, from 4°S to 6°S are green, from 6°S to 8°S are brown, from 8°S to 10°S are grey, from 10°S to 12°S are dark green and from 12°S to 14°S are light blue.

The depth-integrated concentrations of N_2O for the O_2 concentrations of 0-5 µmol kg^{-1}, 5-20 µmol kg^{-1}, 20-63,5 µmol kg^{-1}, and more than 63,5 µmol kg^{-1} are represented in Figure 12. The data is the average of all stations measured during the cruise of each year until a maximum depth of 1000 m, which was chosen to enable a representative comparison for the different cruises as at some stations no samples were taken from a deeper depth. Furthermore, it should be taken into consideration that for some years

more samples were taken at one station with smaller gaps allowing for a more precise placement in the O_2 concentration categories.

For the years 2009, 2015 and 2022 the highest depth-integrated concentration is found with a O_2 concentration between 20 - 63,5 µmol kg^{-1}, for the years 2012 and 2017 it is found with a O_2 concentration between 5 - 20 µmol kg^{-1}. The year 2022 shows the highest overall concentration of N_2O, which could be caused by the differences in the amount of samples that were taken from one station, as in 2022 significantly less samples were taken from one station compared to the other years. For each year except 2015 the concentration of N_2O with a O_2 concentration between 0 - 5 µmol kg^{-1} is less than the concentration of N_2O with a O_2 concentration between 5 - 20 µmol kg^{-1}. The N_2O concentration at a O_2 concentration of more than 63,5 µmol kg^{-1} is for all year significantly smaller than in the other categories.

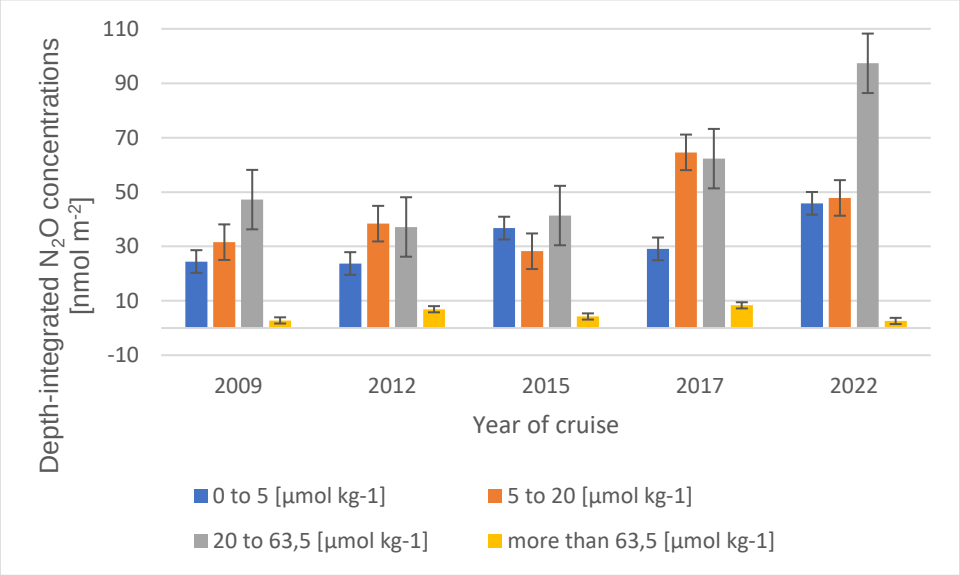

Fig. 12: Comparison of the average depth-integrated N_2O concentrations of the cruises in the years 2009, 2012, 2015, 2017, and 2022. The blue bars show the average concentration of N_2O for an O_2 concentration of 0 - 5 µmol kg^{-1}, orange shows the average concentration of N_2O for an O_2 concentration of 5 - 20 µmol kg^{-1}, grey resembles the concentration of N_2O for an O_2 concentration of 20 - 63,5 µmol kg^{-1} and yellow the N_2O concentration for the O_2 concentration above 63,5 µmol kg^{-1}. The black bar at the top of each column indicates the standard derivation.

4.3.2. Comparison of saturation, average maximum N_2O concentration and depth of maximum N_2O concentration

Saturation is indicating, how much N_2O is in the water compared with the concentration of the atmosphere. Is the saturation 100 % the equilibrium between the water and the atmosphere is reached. Oversaturation indicates outgassing of N_2O towards the atmosphere, whereas undersaturation indicates potential uptake by the ocean. The N_2O saturation of the surface water is calculated with the following equation:

$$\frac{N_2O\ (observed)}{N_2O\ (equilibrium)} \times 100 \qquad (6)$$

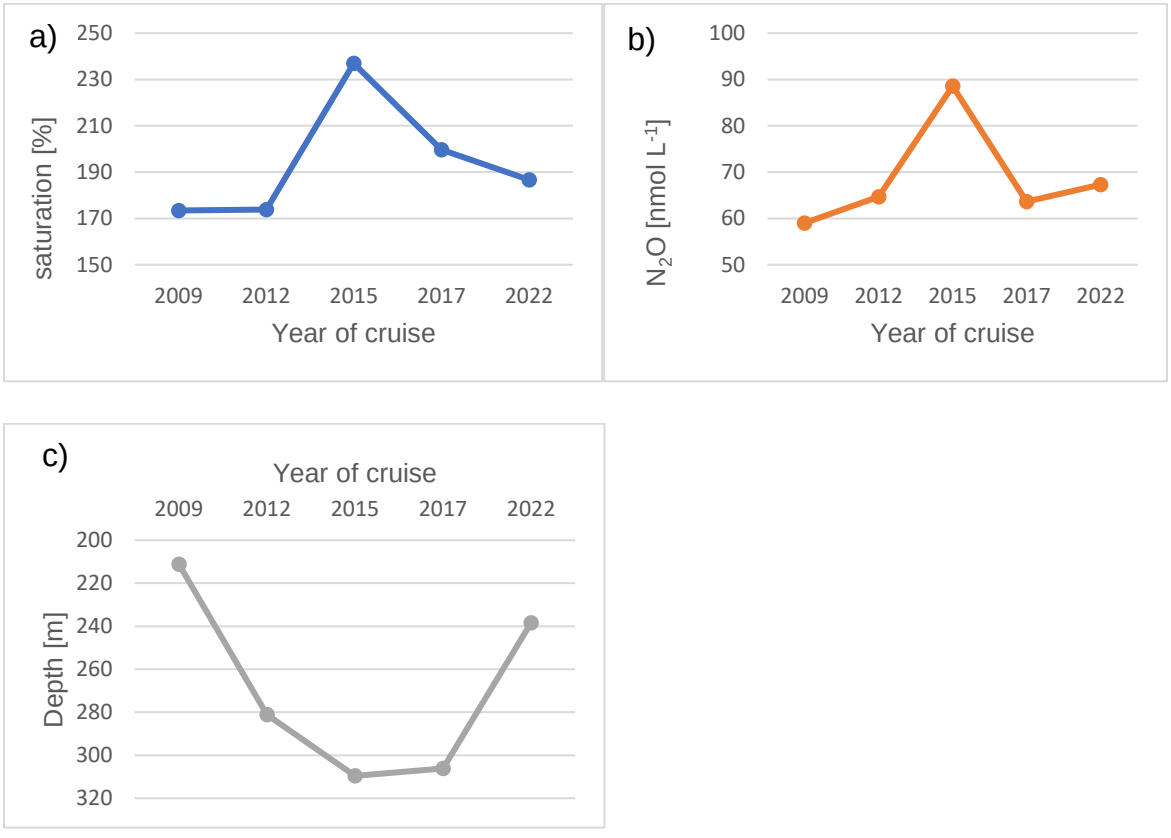

Fig. 13: Showing a) the saturation, b) the average maximum N_2O concentration and c) the average depth of the maximum N_2O concentration for the years 2009, 2012, 2015, 2017 and 2022.

For all the years a saturation over 100 % was found (Figure 13), indicating the concentration of N_2O is higher in the water compared to the atmosphere. For the years 2009 and 2012 a similar saturation of 173 % and 174 % was evaluated. 2015 has the highest saturation of 237 %, for 2017 the saturation is lower (200 %) and for 2022 the saturation is 187 %.

For the maximum concentration of N_2O a similar distribution is visible. For 2015, the strong El Niño year, the highest maximum of 90 µmol L^{-1} can be seen. After 2015 it drops to a similar value as in 2012 and rises to 67 µmol L^{-1} in 2022. The maximum for the N_2O concentration for 2009 is in average 59 µmol L^{-1} and rises about 5 µmol L^{-1} for the year 2012.

The depth of the N_2O maximum is the deepest for 2015 with 309 m followed shortly after by 2017 with 306 m and the lowest in 2009 and 2022 with 211 m and 238 m.

5. Conclusions

The average N_2O concentration maximum for 2022 is found between a depth of 200 m and 300 m with concentrations between 60 nmol L^{-1} and 80 nmol L^{-1}. The O_2 concentration minimum is found at a depth of almost 400 m. The opposite pattern between these two concentrations and the positive linear regression of AOU plotted against ΔN_2O are indicating a N_2O production through nitrification.

The comparison with the archived data shows a clear increase in the N_2O concentration maximum for the year 2015. The maximum was also found at the deepest depth and 2015 holds the highest saturation of 238 %. These are indicators for a connection between the El Niño event and the N_2O concentration in the water column. For the La Niña event the impact on the distribution of N_2O in the water column was less clear. The saturation for 2017 and 2022 were higher than the neutral year 2012, yet 2009 was the same as 2012. The N_2O concentration maxima were showing a similar pattern. The lower linear regression in the AOU plot for 2017, or the negative AOU values in 2009 could be indicators for a La Niña event, yet it is not seen for all years that encountered a La Niña event and, therefore, it could have been influenced by other causes.

For further meaningful findings it should be investigated whether La Niña and neutral years have distinctive features. Furthermore, the El Niño event of 2015 should be compared with more El Niño events to ensure 2015 is not an outlier, but rather a typical distribution of N_2O for these events.

References

Arp, Daniel J. (2009): Nitrification: John Wiley & Sons, Ltd (eLS). Available online at https://onlinelibrary.wiley.com/doi/full/10.1002/9780470015902.a0021154.

Bakker, Dorothee C. E.; Bange, Hermann W.; Gruber, Nicolas; Johannessen, Truls; Upstill-Goddard, Rob C.; Borges, Alberto V. et al. (Eds.) (2014): Air-Sea Interactions of Natural Long-Lived Greenhouse Gases (CO2, N2O, CH4) in a Changing Climate. Berlin, Heidelberg: Springer. Available online at https://library.oapen.org/bitstream/handle/20.500.12657/28060/1001934.pdf?sequence=1#page=165, checked on 7/14/2022.

Cane, Mark A. (1986): El Niño. In *Annual Review of Earth and Planetary Sciences* 14, pp. 43–70. DOI: 10.1146/annurev.ea.14.050186.000355.

Devol, Allan H. (2015): Denitrification, Anammox, and N2 Production in Marine Sediments. In *Annual Review of Marine Science* 7, pp. 403–423. DOI: 10.1146/annurev-marine-010213-135040.

Farías, Laura; Paulmier, Aurélien; Gallegos, Mauricio (2007): Nitrous oxide and N-nutrient cycling in the oxygen minimum zone off northern Chile. In *Deep Sea Research Part I: Oceanographic Research Papers* 54 (2), pp. 164–180. DOI: 10.1016/j.dsr.2006.11.003.

Ji, Qixing; Altabet, Mark A.; Bange, Hermann W.; Graco, Michelle I.; Ma, Xiao; Arévalo-Martínez, Damian L.; Grundle, Damian S. (2019): Investigating the effect of El Niño on nitrous oxide distribution in the eastern tropical South Pacific. In *Biogeosciences* 16 (9), pp. 2079–2093. DOI: 10.5194/bg-16-2079-2019.

José, Yonss Saranga; Stramma, Lothar; Schmidtko, Sunke; Oschlies, Andreas (2019): ENSO-driven fluctuations in oxygen supply and vertical extent of oxygen-poor waters in the oxygen minimum zone of the Eastern Tropical South Pacific. In *Biogeosciences Discussions*, pp. 1–20. DOI: 10.5194/bg-2019-155.

Kock, A.; Arévalo-Martínez, D. L.; Löscher, C. R.; Bange, H. W. (2016): Extreme N2O accumulation in the coastal oxygen minimum zone off Peru. In *Biogeoscience* 13 (3), pp. 827–840.

Kolb, Bruno (2003): Gaschromatographie in Bildern. [eine Einführung ; erw. um GC-MS Kopplung]. 2., überarb. u. erw. Aufl. Weinheim [u.a.]: Wiley-VCH.

Montecino, Vivian; Lange, Carina B. (2009): The Humboldt Current System: Ecosystem components and processes, fisheries, and sediment studies. In *Progress in Oceanography* 83 (1-4), pp. 65–79. DOI: 10.1016/j.pocean.2009.07.041.

Neelin, J. David; Latif, Mojib (1998): El Niño Dynamics. Bringer of storms and droughts, the El Niño/Southern Oscillation results from the complex, sometimes chaotic interplay of ocean and atmosphere. In *American Institute of Physics* 51, pp. 32–36. DOI: 10.1063/1.882496.

Quack, Birgit (2022): Pan-Atlantic connectivity of marine biofeochemical and ecological processes and the impact of anthropogenic pressures. SO287.

Ryabenko, E.; Kock, A.; Bange, H. W.; Altabet, M. A.; Wallace, D. W. R. (2012): Contrasting biogeochemistry of nitrogen in the Atlantic and Pacific Oxygen Minimum Zones. In *Biogeosciences* 9 (1), pp. 203–215. DOI: 10.5194/bg-9-203-2012.

Snow, N. H.; Bullock, G. P. (2010): Novel techniques for enhancing sensitivity in static headspace extraction-gas chromatography. In *Elsevier* (1217), pp. 2726–2735. Available online at https://reader.elsevier.com/reader/sd/pii/S0021967310000166?token=898A7A6736F853144339CC2E167AEE5E8C723B9C980F92F407BED9692AE83825C889E7848E5A301726FD503CD0A935E0&originRegion=eu-west-1&originCreation=20220714093633, checked on 7/14/2022.

Vitha, Mark F. (2016): Chromatography : Principles and Instrumentation. Newark, UNITED STATES: John Wiley & Sons, Incorporated. Available online at http://ebookcentral.proquest.com/lib/christianalbrechts/detail.action?docID=4653434.

Walter, S.; Bange, H. W.; Breitenbach, U.; Wallance, D. W. R. (2006): Nitrous oxide in the North Atlantic Ocean. In *Biogeosciences* 3, pp. 607–619.

Wrage, N.; Velthof, G.L; van Beusichem, M.L; Oenema, O. (2001): Role of nitrifier denitrification in the production of nitrous oxide. In *Soil Biology and Biochemistry* 33 (12-13), pp. 1723–1732. DOI: 10.1016/S0038-0717(01)00096-7.

Appendix

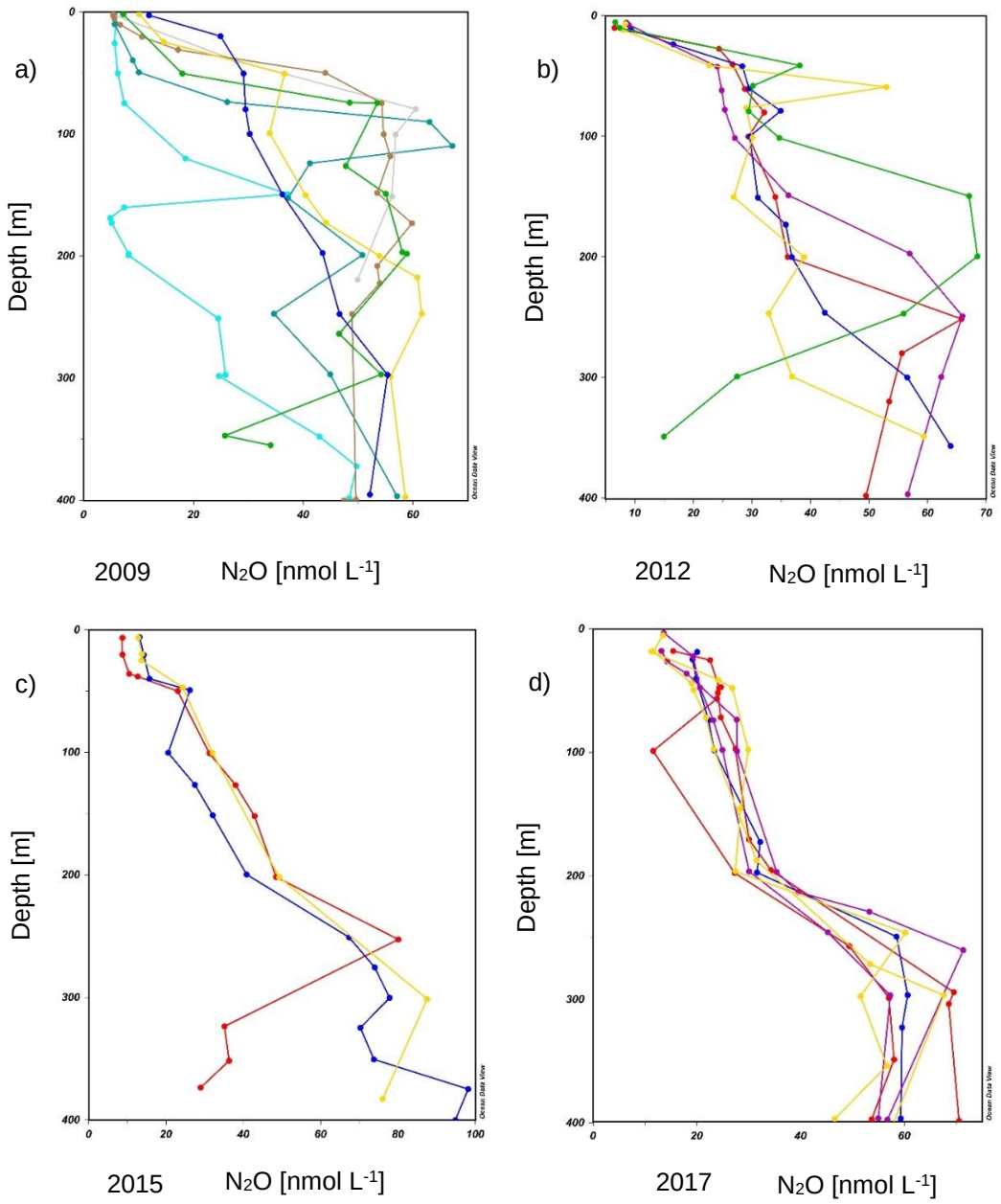

Fig. 14: Depth profiles until a depth of 400 m of the years a) 2009, b) 2012, c) 2015, and d) 2017, showing the N_2O concentration. The stations located in the Latitude section from 2°N to the Equator are red, station located on the Equator are blue, the stations located in the section from the Equator to 2°S are violet, from 2°S to 4°S are yellow, from 4°S to 6°S are green, from 6°S to 8°S are brown, from 8°S to 10°S are grey, from 10°S to 12°S are dark green and from 12°S to 14°S are light blue.

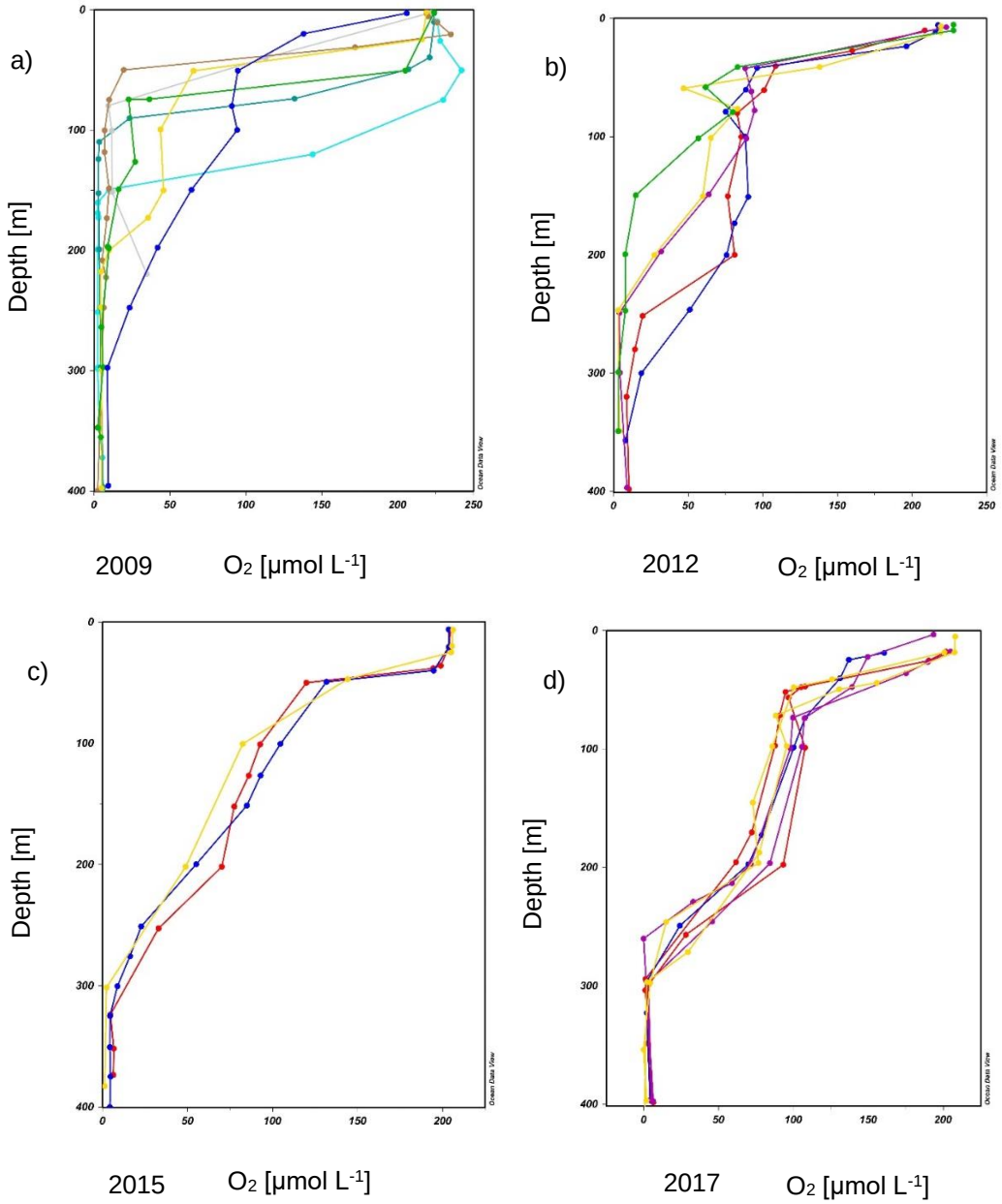

Fig. 15: Depth profiles until a depth of 400 m of the years a) 2009, b) 2012, c) 2015, and d) 2017, showing the O_2 concentration. The stations located in the Latitude section from 2°N to the Equator are red, station located on the Equator are blue, the stations located in the section from the Equator to 2°S are violet, from 2°S to 4°S are yellow, from 4°S to 6°S are green, from 6°S to 8°S are brown, from 8°S to 10°S are grey, from 10°S to 12°S are dark green and from 12°S to 14°S are light blue.

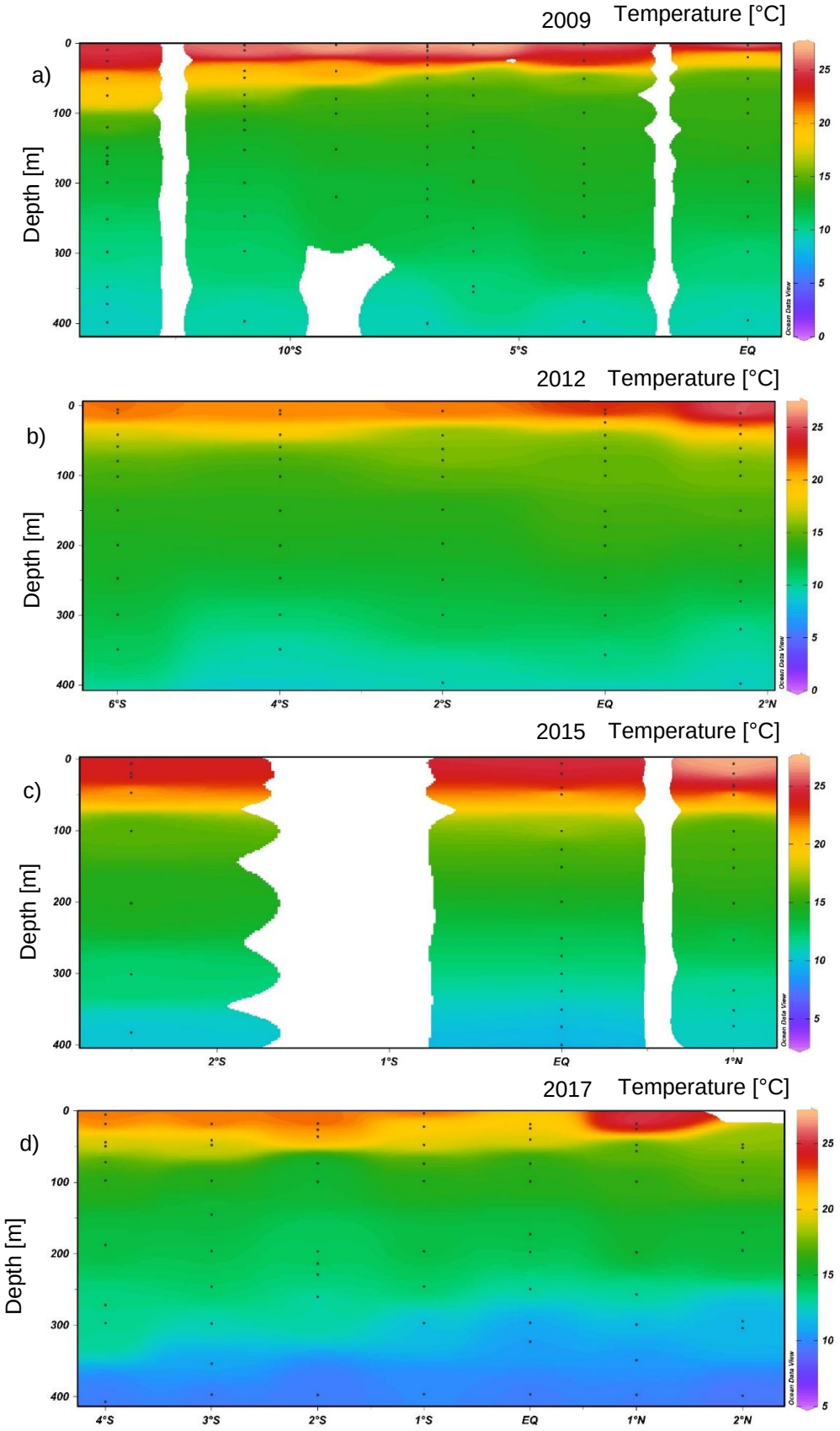

Fig. 16: Vertical sections of the Temperature for the years a) 2009, b) 2012, c) 2015 and d) 2017.

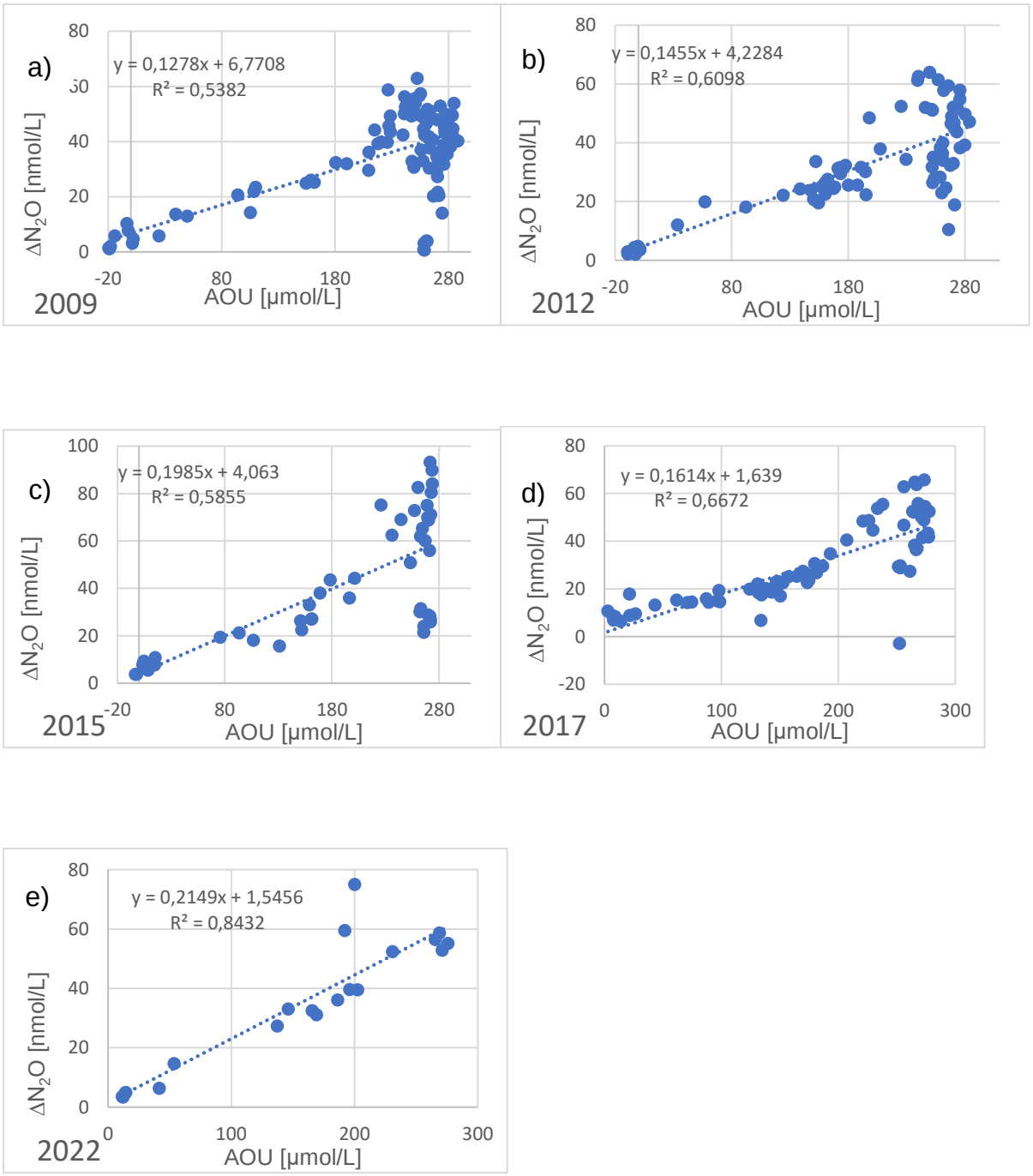

Fig. 17: Plot of AOU and ΔN_2O showing the linear regression for a) 2009, b) 2012, c) 2015, d) 2017 and e) 2022.

Cruise	Station	Sample ID	Depth [m]	Latitude [°N]	Longitude [°W]	N_2O [nmol L^{-1}]	Mean [nmol L^{-1}]
SO287	33	28712099	2845,801	2,26392	-85,83308	17,81	11,14
SO287	33	28712099	2845,801	2,26392	-85,83308	10,54	
SO287	33	28712099	2845,801	2,26392	-85,83308	11,74	
SO287	33	28712101	1997,48	2,26386	-85,83316	8,89	8,20
SO287	33	28712101	1997,48	2,26386	-85,83316	8,73	
SO287	33	28712101	1997,48	2,26386	-85,83316	6,99	
SO287	33	28712103	999,893	2,26394	-85,83318	31,32	59,91
SO287	33	28712103	999,893	2,26394	-85,83318	59,68	
SO287	33	28712103	999,893	2,26394	-85,83318	60,13	
SO287	33	28712106	351,882	2,26398	-85,83314	9,20	9,47
SO287	33	28712106	351,882	2,26398	-85,83314	8,92	
SO287	33	28712106	351,882	2,26398	-85,83314	10,29	
SO287	33	28712110	202,997	2,26396	-85,83316	62,47	57,22
SO287	33	28712110	202,997	2,26396	-85,83316	57,52	
SO287	33	28712110	202,997	2,26396	-85,83316	56,92	
SO287	33	28712114	53,743	2,26392	-85,8332	39,09	35,90
SO287	33	28712114	53,743	2,26392	-85,8332	35,79	
SO287	33	28712114	53,743	2,26392	-85,8332	36,01	
SO287	33	28712116	35,899	2,26398	-85,83316	39,47	35,49
SO287	33	28712116	35,899	2,26398	-85,83316	36,73	
SO287	33	28712116	35,899	2,26398	-85,83316	34,24	
SO287	33	28712121	10,225	2,26398	-85,83316	22,85	24,08
SO287	33	28712121	10,225	2,26398	-85,83316	24,27	
SO287	33	28712121	10,225	2,26398	-85,83316	25,12	
SO287	34	28712139	997,802	0,4535	-85,83298	63,41	63,44
SO287	34	28712139	997,802	0,4535	-85,83298	55,02	
SO287	34	28712139	997,802	0,4535	-85,83298	63,46	
SO287	34	28712144	400,335	0,45334	-85,83294	37,51	37,86
SO287	34	28712144	400,335	0,45334	-85,83294	38,21	
SO287	34	28712144	400,335	0,45334	-85,83294	34,16	
SO287	34	28712146	201,265	0,45348	-85,8329	27,98	27,74
SO287	34	28712146	201,265	0,45348	-85,8329	26,85	
SO287	34	28712146	201,265	0,45348	-85,8329	28,40	
SO287	34	28712150	69,887	0,45347	-85,83292	59,28	57,64
SO287	34	28712150	69,887	0,45347	-85,83292	44,54	
SO287	34	28712150	69,887	0,45347	-85,83292	55,99	
SO287	34	28712154	51,135	0,45342	-85,83294	8,02	8,41
SO287	34	28712154	51,135	0,45342	-85,83294	8,84	
SO287	34	28712154	51,135	0,45342	-85,83294	8,38	
SO287	34	28712158	8	0,45348	-85,83296	41,22	40,92
SO287	34	28712158	8	0,45348	-85,83296	40,61	
SO287	34	28712158	8	0,45348	-85,83296	37,31	
SO287	35	28712176	2395,405	-1,33968	-85,83328	37,89	44,39
SO287	35	28712176	2395,405	-1,33968	-85,83328	45,05	

Cruise	Station	Sample ID	Depth [m]	Latitude [°N]	Longitude [°W]	N_2O [nmol L^{-1}]	Mean [nmol L^{-1}]
SO287	35	28712176	2395,405	-1,33968	-85,83328	43,73	
SO287	35	28712178	1996,149	-1,33962	-85,83332	59,18	61,27
SO287	35	28712178	1996,149	-1,33962	-85,83332	1,54	
SO287	35	28712178	1996,149	-1,33962	-85,83332	63,35	
SO287	35	28712180	998,795	-1,33968	-85,83328	22,21	23,45
SO287	35	28712180	998,795	-1,33968	-85,83328	24,69	
SO287	35	28712180	998,795	-1,33968	-85,83328	27,28	
SO287	35	28712183	331,281	-1,33966	-85,8333	39,51	37,31
SO287	35	28712183	331,281	-1,33966	-85,8333	36,61	
SO287	35	28712183	331,281	-1,33966	-85,8333	38,00	
SO287	35	28712187	201,437	-1,33966	-85,83328	19,44	19,48
SO287	35	28712187	201,437	-1,33966	-85,83328	23,36	
SO287	35	28712187	201,437	-1,33966	-85,83328	19,52	
SO287	35	28712191	52,104	-1,33692	-85,8333	10,01	9,75
SO287	35	28712191	52,104	-1,33962	-85,8333	9,89	
SO287	35	28712193	30,019	-1,33964	-85,83328	32,27	32,09
SO287	35	28712193	30,019	-1,33964	-85,83328	32,60	
SO287	35	28712193	30,019	-1,33964	-85,83328	31,41	
SO287	35	28712198	8,513	-1,33974	-85,8333	25,90	24,85
SO287	35	28712198	8,513	-1,33974	-85,8333	25,91	
SO287	35	28712198	8,513	-1,33974	-85,8333	22,75	
SO287	36	28712209	998,094	-2,66644	-85,83164	45,62	44,37
SO287	36	28712209	998,094	-2,66644	-85,83164	44,54	
SO287	36	28712209	998,094	-2,66644	-85,83164	42,96	
SO287	36	28712214	364,567	-2,66648	-85,83164	56,99	58,28
SO287	36	28712214	364,567	-2,66648	-85,83164	59,09	
SO287	36	28712214	364,567	-2,66648	-85,83164	58,75	
SO287	36	28712216	200,273	-2,66638	-85,83168	63,82	64,25
SO287	36	28712216	200,273	-2,66638	-85,83168	66,30	
SO287	36	28712216	200,273	-2,66638	-85,83168	62,63	
SO287	36	28712219	51,329	-2,66634	-85,83168	81,29	79,84
SO287	36	28712219	51,329	-2,66634	-85,83168	79,47	
SO287	36	28712219	51,329	-2,66634	-85,83168	78,76	
SO287	36	28712224	33,7	-2,66642	-85,83156	63,52	63,72
SO287	36	28712224	33,7	-2,66642	-85,83156	62,88	
SO287	36	28712224	33,7	-2,66642	-85,83156	64,77	
SO287	36	28712228	7,018	-2,6664	-85,83158	62,08	57,52
SO287	36	28712228	7,018	-2,6664	-85,83158	52,95	
SO287	36	28712228	7,018	-2,6664	-85,83158	49,98	

Eigenständigkeitserklärung

Hiermit erkläre ich, dass ich die vorliegende Arbeit eigenständig und ohne fremde Hilfe angefertigt habe und keine anderen als die angegebenen Quellen und Hilfsmittel verwendet habe.
Die eingereichte schriftliche Fassung der Arbeit entspricht der auf dem elektronischen Speichermedium.
Weiterhin versichere ich, dass diese Arbeit noch nicht als Abschlussarbeit an einer anderen Stelle vorgelegen hat.

Datum, Unterschrift